

Comparing roughness descriptors for distinct terrain surfaces in point cloud data

Lei Fan ¹ and Yang Zhao ²

¹ Department of Civil Engineering, Xi'an Jiaotong-Liverpool University, Suzhou, China

² School of Intelligent Manufacturing and Smart Transportation, Suzhou City University, Suzhou, China

Abstract: Terrain surface roughness, often described abstractly, poses challenges in quantitative characterisation with various descriptors found in the literature. This study compares five commonly used roughness descriptors, exploring correlations among their quantified terrain surface roughness maps across three terrains with distinct spatial variations. Additionally, the study investigates the impacts of spatial scales and interpolation methods on these correlations. Dense point cloud data obtained through Light Detection and Ranging technique are used in this study. The findings highlight both global pattern similarities and local pattern distinctions in the derived roughness maps, emphasizing the significance of incorporating multiple descriptors in studies where local roughness values play a crucial role in subsequent analyses. The spatial scales were found to have a smaller impact on rougher terrain, while interpolation methods had minimal influence on roughness maps derived from different descriptors.

Keywords: roughness; digital elevation model; point cloud; terrain; LiDAR; remote sensing

1. Introduction

Terrain surface roughness is a key metric in the earth sciences that describes the complexity or variability of a terrain surface at a specific spatial scale. Its applications include digital terrain analysis, simulation of Earth surface processes, and terrain classification [1]-[6]. Depending on the application requirements, calculations may involve the determination of global or local terrain roughness. Especially when using point cloud data as the main data source, local terrain roughness is often calculated [7]-[11]. This is because such data have fine spatial resolution and can record local topographic surface characteristics and spatial changes in detail. The acquisition of these data is usually achieved through measurement technologies such as Light Detection and Ranging (LiDAR) and Structure from Motion and Multi-View Stereo (SfM-MVS).

There is often ambiguity in the definition of terrain surface roughness. Roughness indicators usually rely on quantitative descriptions of changes in specific terrain features, such as local relief, degree of folds, or the extent of local mutations. Commonly used indicators include but are not limited to root mean square height (RMSH) [11], standard deviation of residual elevation [9], standard deviation of curvature [2], and standard deviation of slope [12]-[13], geostatistical analysis [14] and fractal dimension analysis [15].

Due to the wide range of applications and the diversity of user requirements, a universally accepted or preferred estimation method for terrain surface roughness has not yet been established. In practical applications and research, people usually select one commonly used terrain surface descriptor

based on personal preference, while little consideration is given to the validity of the local roughness map derived for a specific application. For rigorous applications, researchers evaluate multiple roughness descriptors to compare the results of interest to determine a more appropriate descriptor [7]-[11]. The comparison is usually based on simple visual inspection for the particular application under consideration [2], [9]. This approach requires more effort during the data processing stage.

To date, there have been few dedicated studies investigating quantitative correlations between terrain surface roughness metrics, which is the motivation for this study. In this study, a comparative analysis of five commonly used roughness descriptors is performed using three lidar point cloud datasets representing different terrain surface complexities.

2. Materials and Methods

2.1. Study data

This study considers three sets of airborne LiDAR data representing similar-sized pieces of bare earth surface, approximately 350 metres by 350 metres. These three terrain surfaces show distinct spatial variation characteristics: hilly rough terrain (average data spacing is 0.64 metres), flat rough terrain (average data spacing is 0.63 metres) and flat smooth terrain (average data spacing is 0.63 metres). These data are extracted from a large LiDAR data set obtained by the National Airborne Laser Mapping Centre of the USA in a volcanic area in central Nevada [16]- [17].

Each set of point cloud data exhibits a discernible global elevation trend. In order to mitigate its influence on local surface roughness calculations and enhance the visualization of surface spatial variability, the global trend within each set of point clouds is removed by subtracting the corresponding best-fitting plane. Consequently, this process results in a set of residual elevations with a global mean elevation value of zero.

Point cloud data of residual elevations serve as the study data for deriving local surface roughness maps. The left-side plots in Figure 1 depict the detrended point cloud data, with elevation represented by colour. Additionally, the histograms in Figure 1 illustrate the distribution of elevation values, accompanied by the display of the range and the standard deviation of all elevation values. These two statistics provide insights into the overall roughness of the three terrain surfaces under consideration.

2.2. Digital elevation model (DEM) maps

Certain surface roughness descriptors, such as RMSH, are applicable to both unstructured scatter point cloud data and gridded (i.e. structured) data in the form of digital elevation models (DEMs). In contrast, many other descriptors like the standard deviation of slope are typically exclusive to gridded DEM maps.

To ensure a consistent comparison of various metrics for estimating roughness, this study uses gridded DEM maps to calculate local surface roughness. To generate such maps, spatial interpolation is needed to convert scattered elevation data into a grid format. A range of interpolation methods is available, with simpler methods often preferred for high-density point cloud data [4].

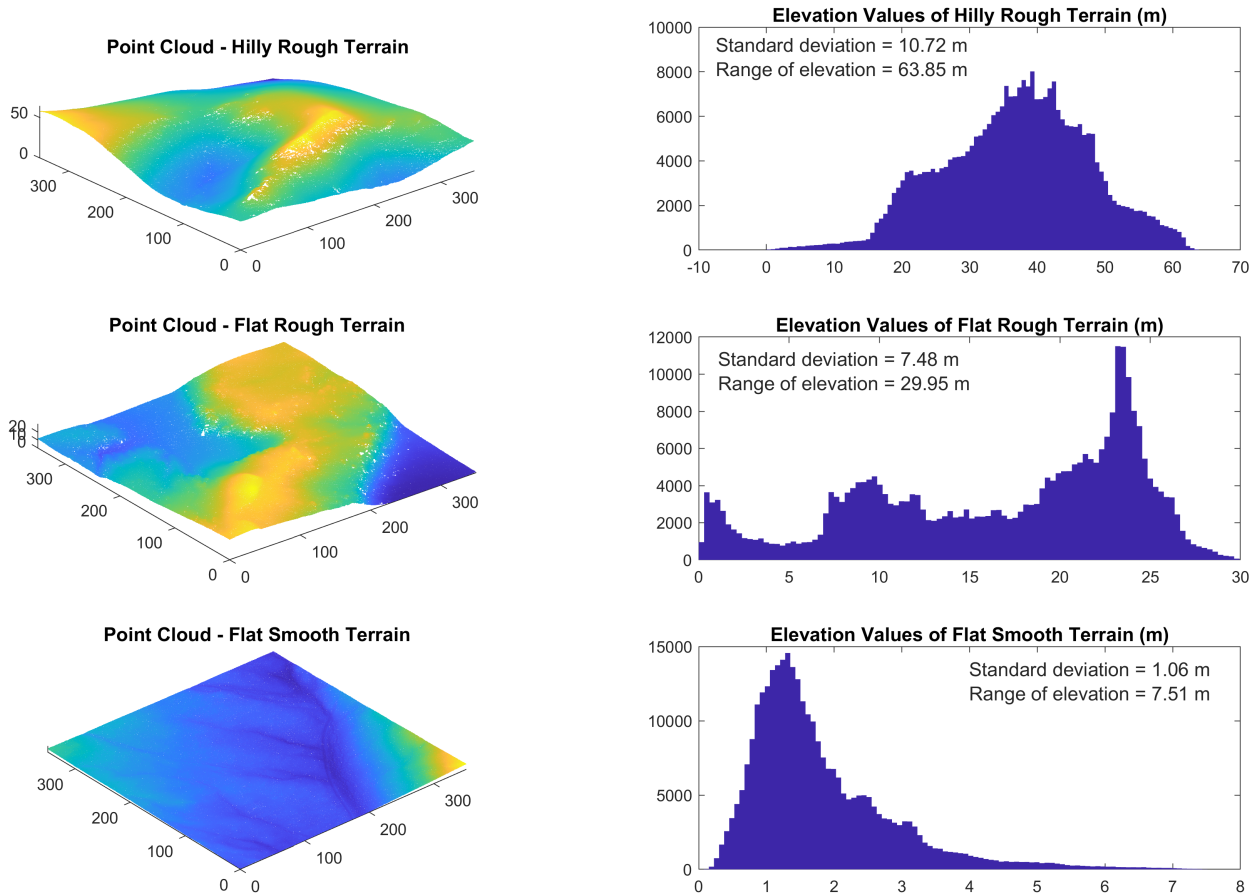


Figure 1. Point cloud data (left) and elevation histograms (right).

To understand the potential impact of interpolation methods on roughness maps generated from different roughness descriptors, this study considers three commonly used interpolation techniques. These include nearest neighbour interpolation (i.e., assigning the elevation value of the nearest known data point to a query grid location), triangulation with linear interpolation (i.e., using the Delaunay triangulation to form triangles, and determining the elevation at a query grid location through linear interpolation using the triangle's three vertices) [18], and natural neighbour interpolation (i.e. identifying the nearest subset of known data points to a query grid location and assigning weights to them according to proportional areas to interpolate a value at the query location). Compared to many other interpolation techniques, these three interpolation methods do not require any user-defined parameters as input and therefore enhance consistency of generated DEM maps. Considering the spatial resolutions of the point cloud data used, a spatial grid resolution of 1 metre is employed for constructing DEM maps in this study.

2.3. Terrain surface roughness descriptors

This study investigates five commonly used descriptors for terrain roughness, with an elaboration of the computational procedures outlined in Section 2.3. These descriptors include RMSH, standard deviation of locally detrended residual elevations (σ_{LDRE}), standard deviation of residual topography (σ_{RT}), standard deviation of slope (σ_{slope}), and standard deviation of curvature ($\sigma_{curvature}$).

2.3.1. RMSH

RMSH is a frequently used descriptor for quantifying local surface roughness in the context of scattered elevation data [2], [11], [19]. It is also applicable to grided elevation data in a DEM. The definition of RMSH is given in (1).

$$\text{RMSE} = \sqrt{\frac{\sum_{i=1}^n (Z_i - \bar{Z})^2}{n-1}} \quad (1)$$

where n represents the number of the data points selected; Z_i is the elevation value of the i^{th} data point; \bar{Z} is the mean elevation value of all (n) data points selected.

2.3.2. Standard deviation of locally detrended residual elevations

This method involves the linear detrending of local elevation data within a moving window. A best-fitting plane is applied to obtain residual elevation values, and the standard deviation of these residuals in the moving window is computed to represent local surface roughness.

2.3.3. Standard deviation of residual topography

Residual topography is defined as the difference between the original topography (original DEM) and the smoothed topography (smoothed DEM) [9]. In this study, the elevation value at a grid location of the smoothed DEM is determined by averaging the elevation values of its neighboring cells in a 5×5 moving window. As the original and the smoothed DEMs have the same spatial resolution, the residual topography is obtained by the arithmetic subtraction of the elevation values of the corresponding cells of the two DEMs. The standard deviation of the residual topography is calculated to as an indicator of terrain roughness.

2.3.4. Standard deviation of slope

Calculating the standard deviation of slope requires the computation of slope values. Slope represents the rate of change of terrain elevations and is expressed in (2).

$$\text{slope} = \tan^{-1} \left(\sqrt{\left(\frac{dz}{dx}\right)^2 + \left(\frac{dz}{dy}\right)^2} \right) \quad (2)$$

where dz/dx and dz/dy represent the rate of change in the x and the y directions, respectively, for the cell of interest.

In the context of DEM maps, slope is often determined using elevation values in a 3×3 moving window, as shown in (3). dz/dx and dz/dy for the central cell (Z_5) are calculated using (4) and (5), respectively, in which L represents the cell size. When there are cells in the neighbourhood (e.g. at the edge of a DEM) that do not contain elevation data, those cells are assumed to take the elevation

value of the central cell. This is useful for the cells at the edge of a DEM raster to ensure that the slope map has the same spatial extent as the DEM map.

$$\text{Moving Window} = \begin{bmatrix} Z_1 & Z_2 & Z_3 \\ Z_4 & Z_5 & Z_6 \\ Z_7 & Z_8 & Z_9 \end{bmatrix} \quad (3)$$

$$\frac{dz}{dx} = \frac{[(Z_3 + 2Z_6 + Z_9) - (Z_1 + 2Z_4 + Z_7)]}{8L} \quad (4)$$

$$\frac{dz}{dx} = \frac{[(Z_7 + 2Z_8 + Z_9) - (Z_1 + 2Z_2 + Z_3)]}{8L} \quad (5)$$

2.3.5. Standard deviation of curvature

Curvature is determined by computing the second derivative of a DEM map, using the same moving window as employed for slope calculation. Various methods are available for calculating curvature. This study adopts the method proposed by Zevenbergen and Thorne [20]-[21], described in (6) - (8). Similar to slope calculation, non-value cells in the neighborhood are assumed to take the elevation value of the central cell. Once the curvature map is derived, the standard deviation of curvature is calculated to characterise terrain roughness.

$$\text{curvature} = 2E + 2D \quad (6)$$

where D and E are given in (7) and (8), respectively, using the elevation values within the moving window shown in (3).

$$D = \frac{[(Z_4 + Z_6)/2 - Z_5]}{L^2} \quad (7)$$

$$E = \frac{[(Z_2 + Z_8)/2 - Z_5]}{L^2} \quad (8)$$

2.4. Correlation between roughness maps

To assess the correlation between roughness maps, this study computes the correlation coefficient (r) of the pixel values of two maps compared, using (9), which is widely used for assessing correlation between images. A correlation coefficient of 1 represents that the pixel values of two compared maps are perfectly matched at all pixel locations. A correlation coefficient of 0 suggests that the pixel values in one map are randomly different from the corresponding pixel values in the other map.

$$r = \frac{\sum_m \sum_n (A_{mn} - \bar{A})(B_{mn} - \bar{B})}{\sqrt{\left(\sum_m \sum_n (A_{mn} - \bar{A})^2\right)\left(\sum_m \sum_n (B_{mn} - \bar{B})^2\right)}} \quad (9)$$

where A and B represent pixel values of two roughness maps compared, respectively; the subscript m and n refer to the pixel location in the maps; \bar{A} and \bar{B} represent the mean value.

2.5. The spatial scale for local terrain surface roughness

Local terrain surface roughness is often determined at a particular user-defined spatial scale. This is typically implemented using non-overlapping moving windows, in the context of DEM maps. However, the impact of spatial scale on the correlation between roughness maps characterised by different roughness descriptors remains uncertain. Therefore, this study investigates a range of non-overlapping moving window sizes, including 3×3 , 5×5 , 7×7 , 9×9 and 11×11 moving windows, to examine their potential influence.

3. Results

3.1. DEM maps

Figure 2 illustrates the DEM maps produced through the utilisation of detrended point cloud data, employing triangulation with liner interpolation. The DEM maps from the alternative two methods considered are not shown since there are virtually no discernible visual distinctions. This aligns with expectations, as the impact of interpolation methods on DEM maps is typically minimal when applied to highly dense point cloud data. Unless explicitly specified, subsequent analysis results corresponded to the DEM maps derived from triangulation with liner interpolation. The only exception is the case (Section 3.4) where the influence of interpolation methods on the correlations between roughness maps, generated by different roughens descriptors, is under consideration.

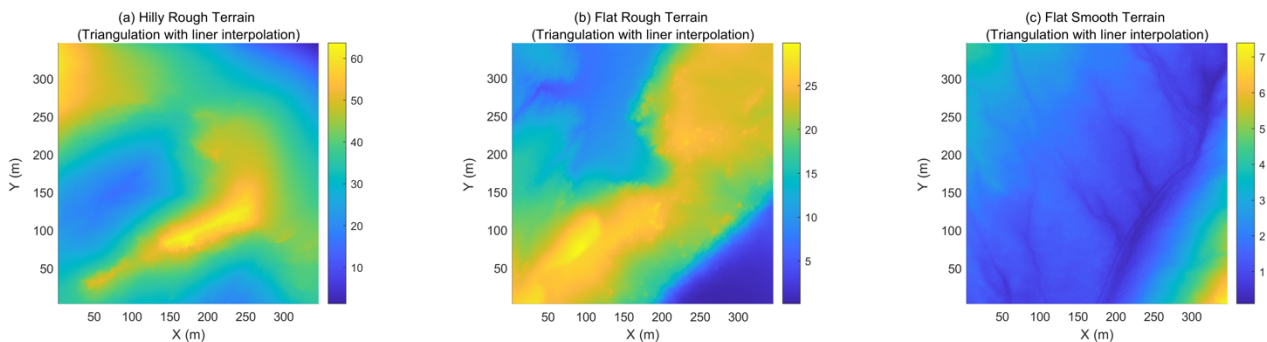


Figure 2. DEM maps of the globally detrended point cloud data: (a) hilly rough terrain, (b) flat rough terrain and (c) flat smooth terrain, using triangulation with liner interpolation.

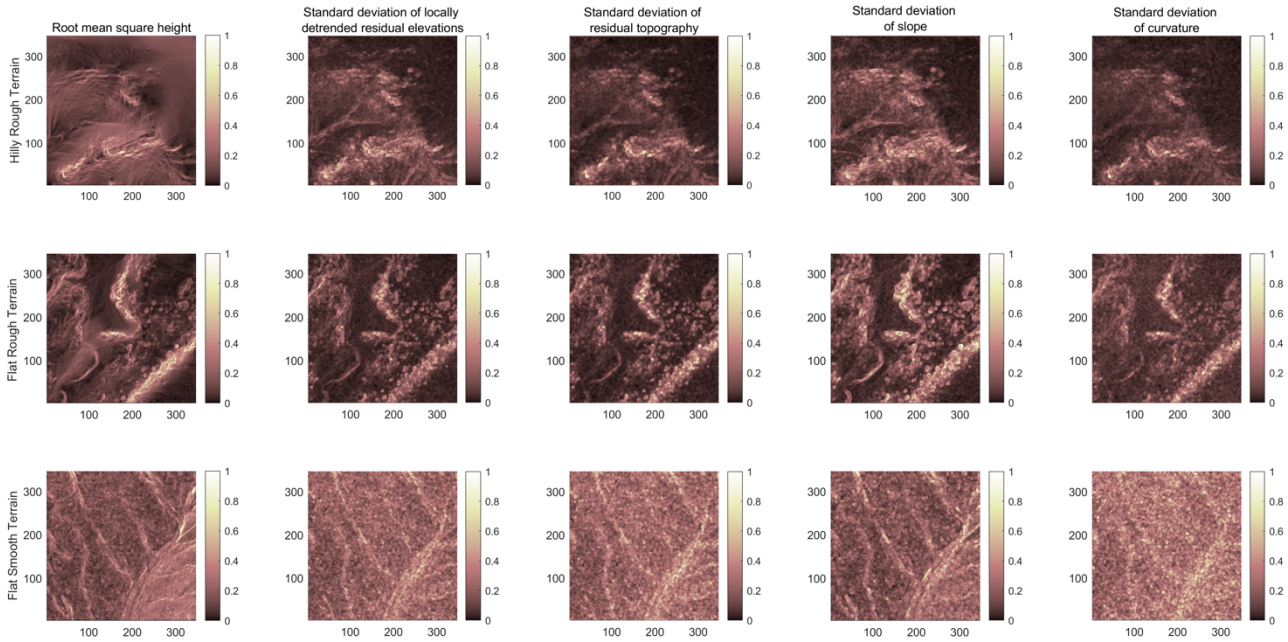


Figure 3. Local roughness maps for the three terrain surfaces, derived using the DEM maps in Figure 2.

3.2. Comparisons on roughness maps

Figure 3 depicts local terrain roughness maps for the five roughness descriptors, utilising a spatial scale of 5×5 cells (a commonly used spatial scale in practice) as an illustrative example. In Figure 3, each column in the plots represents a different roughness descriptor while each row corresponds to one of the three considered terrain surfaces. To enhance visual comparison, the roughness values shown in Figure 3 were normalized to a range of 0 to 1.

Observations revealed that most roughness descriptors produced local terrain roughness maps exhibiting similar global patterns, justifying their widespread use in the literature. Comparatively, the terrain roughness maps produced by RMSH appeared to be more distinct from the others. To verify these observations, the correlation coefficient r for each pair of compared roughness maps was calculated using (8) for the three terrain surfaces considered. With five roughness descriptors in consideration, a total of 10 pairs were formed for comparison. The correlation coefficient values are visually presented in the radar charts depicted in Figure 4. In these radar charts, each vertex corresponds to a roughness descriptor, and markers along each axis from the radar centre (where $r = 0$) to the vertex (where $r = 1$) represent the correlation coefficient values between other descriptors and the one located at the vertex.

In the case of rough terrain surfaces (both hilly rough and flat rough), large correlations were identified between roughness maps derived using the considered descriptors, with the exception of RMSH, as shown in Figure 4. Notably, the largest correlation values (approximately 0.963 for hilly rough terrain and 0.957 for flat rough terrain) were observed for the pair σ_{RT} and $\sigma_{curvature}$, aligning with the global patterns of the roughness maps shown in Figure 3 for these two descriptors.

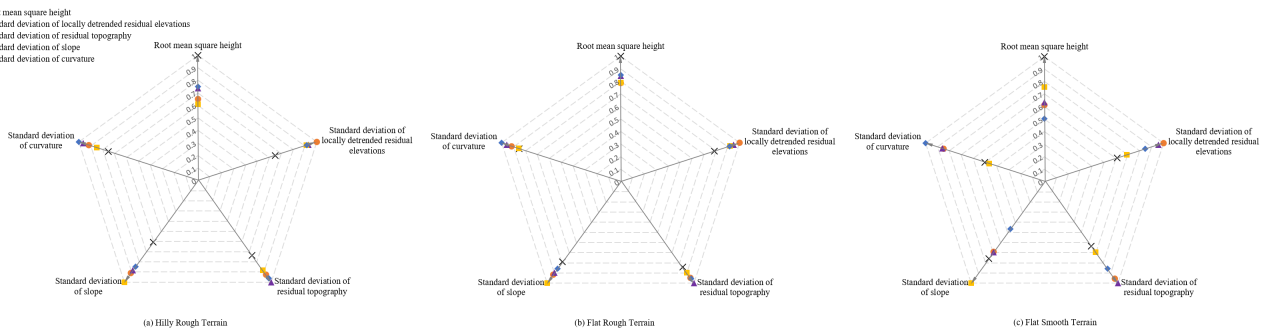


Figure 4. Correlation coefficient values for paired roughness maps. In the charts, each vertex corresponds to a roughness descriptor, and markers along each axis from the radar centre to the vertex represent the correlation coefficient values between other descriptors and the one located at the vertex.

Overall, the correlation coefficient values for the flat rough terrain were found to surpass those for the hilly rough terrain. This was likely attributable to distinct characteristics in the spatial variations between the two terrain surfaces. For the hilly rough terrain, its spatial variation comprised a strong signal spatial variation (as indicated by “hilly”), alongside a noisy spatial variation. In contrast, the flat rough terrain was predominately featured by noisy spatial variations with minimal signal spatial variations (as indicated by “flat”). The characterisation of the signal component likely varied with algorithms (i.e. roughness descriptors in this study), resulting in greater differences between roughness maps produced across different roughness descriptors. For the flat smooth terrain, weak correlations between different roughness descriptors were observed. Generally, the similarity between roughness maps generated by different descriptors was influenced by the magnitude and type of spatial variations. Greater similarity was observed for rougher terrain surfaces, especially those with noisy spatial variations.

The correlation between RMSH and any one of the other four roughness descriptors was observed to be relatively modest, as illustrated in Figure 4. This observation was also supported by the roughness maps presented in Figure 3. It is interesting to observe in Figure 3 that the roughness values of RMSH exhibited greater spatial coherence compared to those derived from the other descriptors. This phenomenon can likely be attributed to the presence of local elevation trends, resulting in stronger local spatial autocorrelation in the RMSH maps. This explanation can be justified by the roughness map of σ_{LDRE} , which shares the same algorithm as RMSH but uses locally detrended elevation values.

Figure 3 further illustrates the presence of local variations in the distributions of roughness values among different descriptors. Certain descriptors (e.g. σ_{RT} and $\sigma_{curvature}$) exhibited similar local distributions, while others (e.g. RMSH and σ_{slope}) were notably different. These distinctions between descriptors imply that the choice of roughness descriptors can impact the results of subsequent analyses, particularly in quantitative studies reliant on local roughness values. As such, it is advisable to carry out a sensitivity analysis using multiple roughness descriptors in quantitative studies where local roughness values are the critical inputs.

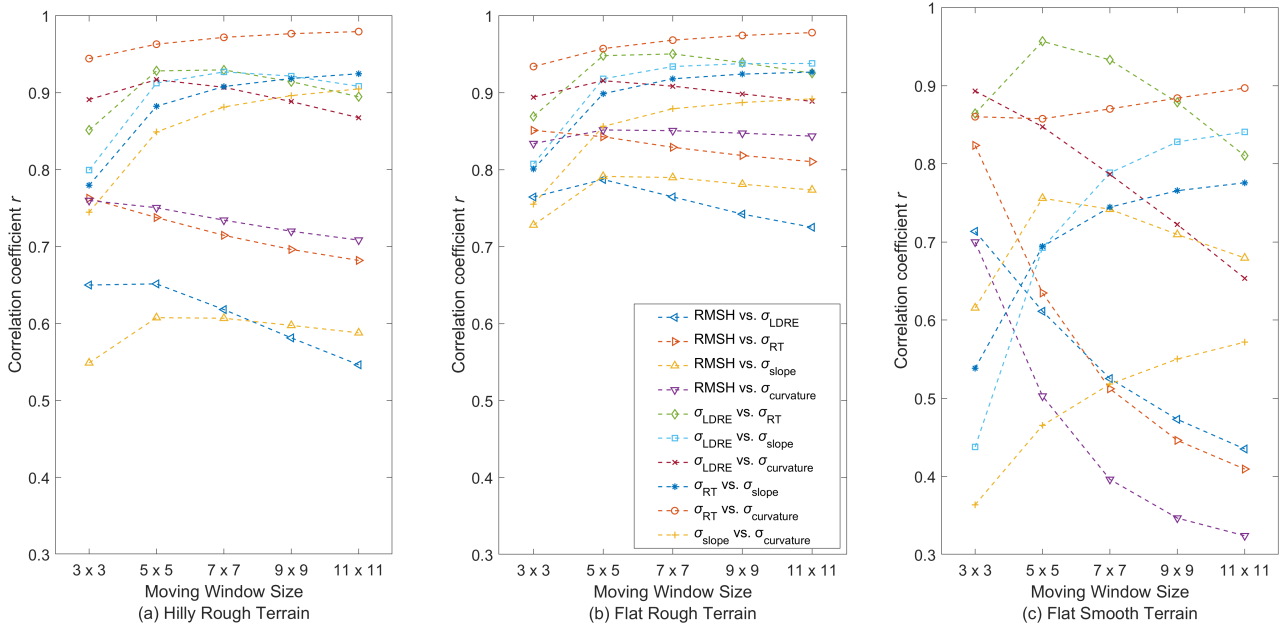


Figure 5. Correlation between paired roughness maps under different window sizes: (a) hilly rough terrain, (b) flat rough terrain, (c) flat smooth terrain.

3.3. Impact of spatial scales

The influence of spatial scales, represented by the moving window size used, on the correlations between roughness maps produced by different roughness descriptors are shown in Figure 5. A mixed behaviour was observed. For the pairs of roughness descriptors compared, a larger window size could either increase or decrease their correlations. Notably, the terrain complexities exerted a great impact, as evidenced by the results presented in Figure 5. The changes of correlation coefficient values with varying spatial scales were significant for the flat smooth terrain. However, for the flat rough terrain, such changes were relatively small for most paired descriptors. This seems to suggest that the impact of the window size on correlations was smaller for the rougher terrain surfaces, especially those characterised by greater noisy spatial variations, such as the flat rough terrain.

3.4. Impact of interpolation methods

The impact of interpolation methods on roughness maps generated from various roughness descriptors is illustrated in Figure 6. Neglectable differences were observed between roughness maps from DEMs through triangulation with linear interpolation and natural neighbour interpolation, as evidenced by significantly large correlation coefficient values. In comparison, roughness maps derived from DEMs through nearest neighbour were slightly more distinct from those from DEMs through triangulation with linear interpolation, especially for the flat smooth terrain. These observations suggest that the influence of interpolation methods on roughness maps derived from different roughness descriptors is minimal, likely attributed to the high-density point cloud data used.

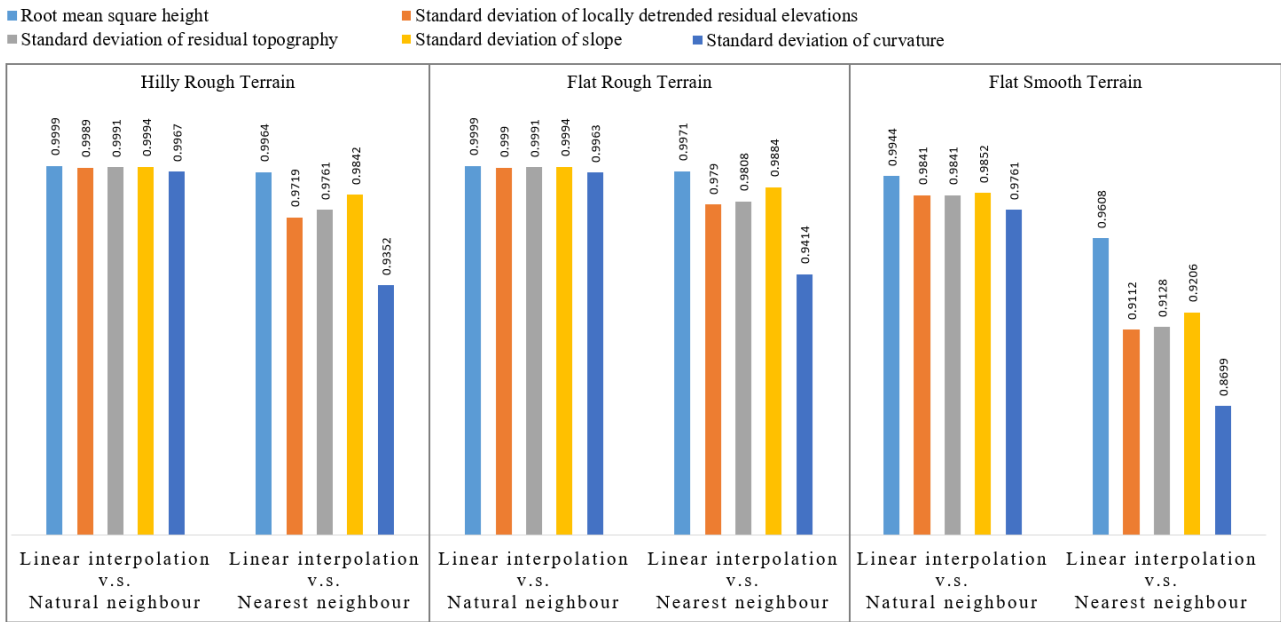


Figure 6. Correlation coefficient values for compared roughness maps from different interpolation methods.

4. Conclusions

This study compared the terrain surface roughness maps quantified by five commonly used roughness descriptors, and explored the correlations of roughness maps produced by these descriptors, for three terrain surfaces of distinct spatial variations. The following findings are found.

1. Local roughness maps from the considered descriptors exhibited similar global patterns across varying spatial complexities, demonstrating their effectiveness in characterizing terrain surface roughness.
2. Similarity between roughness maps generated by different descriptors was influenced by the magnitude and type of spatial variations, with greater similarity observed for rougher terrain surfaces, particularly those with noisy spatial variations.
3. Variations in local distributions of roughness values were noted among descriptors, highlighting the importance of considering multiple descriptors in studies where local roughness values are the input for subsequent analyses, especially for the widely used RMSH, which showed small correlations with the other descriptors.
4. Investigation of the spatial scale of roughness maps revealed mixed effects on correlations between two roughness descriptors, with a smaller impact on correlations for rougher terrain surfaces, especially those with greater noisy spatial variations like the flat rough terrain.
5. Minimal influence of interpolation methods on roughness maps derived from different descriptors was observed, likely due to the high density of the point cloud data used.

Acknowledgments

The author is grateful for the financial support from Xi'an Jiaotong–Liverpool University, which includes the Research Enhancement Fund (grant number REF-21-01-003).

References

1. J. A. Fernando, A. Francisco, A. A. Manuel and C. Fernando, “Effects of terrain morphology, sampling density, and interpolation methods on grid DEM accuracy,” *Photogrammetric Engineering & Remote Sensing*, vol. 71(7), pp. 805-816, 2005. doi:10.14358/pers.71.7.805
2. C. H. Grohmann, M. J. Smith, and C. Riccomini, “Multiscale analysis of topographic surface roughness in the Midland Valley, Scotland,” *IEEE Transactions on Geoscience and Remote Sensing*, vol. 49(4), pp. 1200-1213, 2011. doi:10.1109/tgrs.2010.2053546
3. J. B. Peter, H. S. Vernon, S. Jiro and J. L. Stephen, “Methods for Remote Engineering Geology Terrain Analysis in Boreal Forest Regions of Ontario, Canada,” *Environmental and Engineering Geoscience*, vol. 10(3), pp. 229-241, 2004. doi:10.2113/10.3.229
4. L. Fan and P. M. Atkinson, “Accuracy of digital elevation models derived from terrestrial laser scanning data,” *IEEE Geoscience and Remote Sensing Letters*, vol. 12(9), pp. 1923-1927, 2015, doi: 10.1109/LGRS.2015.2438394
5. L. Fan, *Uncertainty in terrestrial laser scanning for measuring surface movements at a local scale*. University of Southampton: Southampton, UK, 2014.
6. L. Fan, W. Powrie, J. A. Smethurst, P. M. Atkinson and H. Einstein, “The effect of short ground vegetation on terrestrial laser scans at a local scale,” *ISPRS Journal of Photogrammetry and Remote Sensing*, vol.95, pp. 42-52, 2014. doi: 10.1016/j.isprsjprs.2014.06.003
7. K. L. Frankel and J. F. Dolan, “Characterizing arid region alluvial fan surface roughness with airborne laser swath mapping digital topographic data,” *Journal of Geophysical Research F*, vol. 112(2), Article ID F02025, 2007. doi: 10.1029/2006JF000644
8. J. M. Nield and G. F. S. Wiggs, “The application of terrestrial laser scanning to aeolian saltation cloud measurement and its response to changing surface moisture,” *Earth Surf. Processes Landforms*, vol. 36(2), pp. 273-278, 2011. doi:10.1002/esp.2102
9. M. B. Kristen, L. M. Wayne, J. D. Patrick, A. M. Douglas and W. B. Elizabeth, “The Use of LiDAR Terrain Data in Characterizing Surface Roughness and Microtopography,” *Applied and Environmental Soil Science*, vol. 2013, pp. 1–13, 2013. doi:10.1155/2013/891534
10. M. Milenković, N. Pfeifer and P. Glira, “Applying Terrestrial Laser Scanning for Soil Surface Roughness Assessment,” *Remote Sensing*, vol. 7, pp. 2007-2045, 2015. doi: 10.3390/rs70202007
11. L. Fan, “A comparison between structure-from-motion and terrestrial laser scanning for deriving surface roughness: A case study on a sandy terrain surface,” *The International Archives of Photogrammetry, Remote Sensing and Spatial Information Sciences*, vol. 42, pp. 1225-1229, 2020. doi: 10.5194/isprs-archives-XLII-3-W10-1225-2020
12. M. N. Joanna and F. S. W. Giles, “The application of terrestrial laser scanning to aeolian saltation cloud measurement and its response to changing surface moisture,” *Earth Surface Processes and Landforms*, vol. 36(2), pp. 273-278, 2010. doi:10.1002/esp.2102

-
13. L. F. Kurt and F. D. James, "Characterizing arid region alluvial fan surface roughness with airborne laser swath mapping digital topographic data," *Journal of Geophysical Research*, vol. 112(F2), pp. 1-14, 2007. doi:10.1029/2006jf000644
 14. C. H. Huang and J. M. Bradford, "Applications of a Laser Scanner to Quantify Soil Microtopography," *Soil Science Society of America Journal*, vol. 56(1), 14, 1992. doi: 10.2136/sssaj1992.03615995005600010002x
 15. R. Andrle and A. D. Abrahams, "Fractal techniques and the surface roughness of talus slopes," *Earth Surface Processes and Landforms*, vol. 14(3), pp. 197–209, 1989. doi:10.1002/esp.3290140303
 16. L. Fan and P. M. Atkinson, "An Iterative Coarse-to-Fine Sub-Sampling Method for Density Reduction of Terrain Point Clouds," *Remote Sensing*, vol. 11(8), pp. 947, 2019. doi: 10.3390/rs11080947
 17. LiDAR data access was based on [LiDAR, ground] services provided by the OpenTopography Facility. Lidar data acquisition completed by the National Centre for Airborne Laser Mapping. Available from: <https://doi.org/10.5069/G9PR7SX0>
 18. L. Fan, J. A. Smethurst, P. M. Atkinson and W. Powrie, "Propagation of vertical and horizontal source data errors into a TIN with linear interpolation," *International Journal of Geographical Information Science*, vol. 28(7), pp. 1378-1400, 2014. doi: 10.1080/13658816.2014.889299
 19. L. Fan and P. M. Atkinson, "A new multi-resolution based method for estimating local surface roughness from point clouds," *ISPRS Journal of Photogrammetry and Remote Sensing*, vol. 144, pp. 369–378, 2018. doi:10.1016/j.isprsjprs.2018.08.003
 20. L. W. Zevenbergen and C. R. Thorne, "Quantitative analysis of land surface topography," *Earth Surface Processes and Landforms*, vol. 12(1), pp. 47–56, 1987. doi:10.1002/esp.3290120107
 21. I. D. Moore, R. B. Grayson and A. R. Ladson, A. R., "Digital terrain modelling: A review of hydrological, geomorphological, and biological applications," *Hydrological Processes*, vol. 5(1), pp. 3–30, 1991. doi: 10.1002/hyp.3360050103